Catalytic Ignition and Upstream Reaction Propagation in Monolith Reactors

Peter M. Struk[1] and Daniel L. Dietrich[2]
NASA Glenn Research Center, Cleveland, Ohio, 44135

Fletcher J. Miller[3]
National Center for Space Exploration Research, Cleveland, Ohio, 44135

and

James S. T'ien[4]
Case Western Reserve University, Cleveland, Ohio, 44106

Using numerical simulations, this work demonstrates a concept called "back-end ignition" for lighting-off and pre-heating a catalytic monolith in a power generation system. In this concept, a downstream heat source (e.g. a flame) or resistive heating in the downstream portion of the monolith initiates a localized catalytic reaction which subsequently propagates upstream and heats the entire monolith. The simulations used a transient numerical model of a single catalytic channel which characterizes the behavior of the entire monolith. The model treats both the gas and solid phases and includes detailed homogeneous and heterogeneous reactions. An important parameter in the model for back-end ignition is upstream heat conduction along the solid. The simulations used both dry and wet CO chemistry as a model fuel for the proof-of-concept calculations; the presence of water vapor can trigger homogenous reactions, provided that gas-phase temperatures are adequately high and there is sufficient fuel remaining after surface reactions. With sufficiently high inlet equivalence ratio, back-end ignition occurs using the thermophysical properties of both a ceramic and metal monolith (coated with platinum in both cases), with the heat-up times significantly faster for the metal monolith. For lower equivalence ratios, back-end ignition occurs without upstream propagation. Once light-off and propagation occur, the inlet equivalence ratio could be reduced significantly while still maintaining an ignited monolith as demonstrated by calculations using complete monolith heating.

Nomenclature

a*	=	ratio of catalytic to geometric surface area
A	=	channel open flow area (m^2)
A_S	=	solid cross-sectional area (m^2)
C_P	$= \sum_{k=1}^{Kg} C_{P,k} Y_k$	; mean gas specific heat at constant pressure (J / kg /K)
$C_{P,k}$	=	species k gas specific heat at constant pressure (J / kg /K)
C_S	=	solid specific heat (J / kg /K)
D_{km}	=	species k diffusion coefficient into mixture (m^2/s)
h_k	=	enthalpy of species k (J/kg)
h_{Dk}	=	convection mass transfer coefficient for specie k in bulk mixture (m/s)
h_T	=	internal convection heat transfer coefficient (W / m^2·K)

[1] Aerospace Engineer, Combustion & Reacting Systems Branch, 21000 Brookpark Rd., MS 110-3.
[2] Aerospace Engineer, Combustion & Reacting Systems Branch, 21000 Brookpark Rd., MS 110-3.
[3] Principal Researcher, 21000 Brookpark Rd., MS 110-3.
[4] Professor, Mechanical & Aerospace Engineering, 10900 Euclid Ave, Associate Fellow.

k	=	species index
K	=	$K_g + K_S$; total number of species (gas + surface)
k_{fi}	=	forward rate constant for the *i*th reaction (units m, mole, s)
K_g	=	number of gas-phase species
k_{ri}	=	reverse rate constant for the *i*th reaction (units m, mole, s)
k_S	=	thermal conductivity of solid (J/m/s/K)
K_S	=	number of surface species
$\dot{m}$	=	mass flow rate down the channel (kg/s)
n_g	=	number of gas-phase reactions
n_S	=	number of surface reactions
Nu_U	=	Upstream face Nusselt number for monolith
q_i	=	rate of progress of the i^{th} gas reaction (mole / m^3 /s) or rate of progress of the i^{th} surface reaction (mole / m^2 /s)
R_U	=	universal gas-constant (8.314 J / mol / K)
$\dot{s}_k$	=	net production rate of specie k due to all surface reactions (mole / m^2 /s)
S	=	circumferential length of channel cross section = πd (m) or; surface area per unit length (m)
t	=	time (s)
Δt	=	time integration between successive gas-phase integrations (s)
T	=	bulk gas temperature (K)
T_k'	=	temperature of species k entering or leaving control volume (if $\dot{s}_k > 0$ then $T_k' = T_S$ otherwise $T_k' = T$)
T_S	=	solid temperature (K)
u	=	average (bulk) velocity of flow (m/s)
W_k	=	molecular weight of specie k (g/mole)
$\overline{W}$	=	$\left(\sum_{k=1}^{K_g} Y_k / W_k\right)^{-1}$; mean molecular weight of the mixture (g/mole)
x	=	axial coordinate from channel inlet (m)
$[X_k]$	=	molar concentration of specie k (mole / m^3)
Y_k	=	mass fraction of specie k in the bulk mixture
Y_{kW}	=	mass fraction of specie k at the wall
Z_k	=	site fraction of surface specie k

Greek Letters

Γ	=	surface density of site on solid (2.7063 x 10^{-5} mol / m^2 for platinum)
ν_{ki}	=	net stoichiometric coefficient of the k^{th} specie in the *i*th reaction;
ν'_{ki}	=	stoichiometric coefficient of the k^{th} reactant specie in the *i*th reaction
ν''_{ki}	=	stoichiometric coefficient of the k^{th} product specie in the *i*th reaction
ρ	=	mass density of gas (kg/m^3)
ρ_S	=	mass density of solid (kg/m^3)
σ_k	=	site occupancy number - number of sites that species k occupies on surface
ϕ	=	equivalence ratio
$\dot{\omega}_k$	=	gas-phase production rate of specie k due to all gas reactions (mole/m^3/s)

I. Introduction

Catalytic combustion has long been recognized for its potential to reduce temperatures of power generation devices in both large and small scale applications including microcombustors. Such power generation devices often use a channel geometry (or multiple channels such as in a monolith structure) coated with a catalyst through which flows a pre-mixed combustible gas mixture. The catalyst must be at an elevated temperature to initiate a reaction. One challenge for such devices is the startup, or light-off, from a cold initial condition. We propose a new concept for the light-off of a catalytic monolith utilizing a "back-end" ignition scheme. In this concept, only a small portion of the downstream catalyst section is heated (via a gaseous flame stabilized downstream of the monolith or

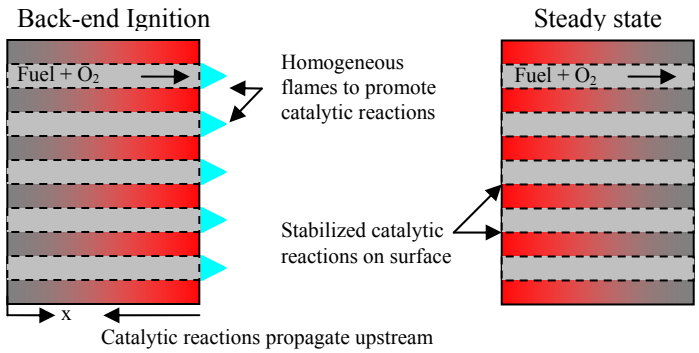

Figure 1. Back-end ignition concept for monolith reactor using downstream homogeneous flame.

Joule heating of the solid) initiating a localized catalytic reaction (see Fig. 1). The catalytic reaction releases sufficient heat which is conducted upstream via the solid causing the reaction zone to propagate, ultimately heating the entire monolith. Recently, we have predicted such a phenomenon using a numerical model and verified the predictions with an experiment in an isolated non-adiabatic single tube made of pure platinum.[1-3]

In this work, we utilize the same numerical model, which is of a transient catalytic channel, but extend the results to a monolith configuration. The fuel used for the simulation is premixed carbon monoxide in air. CO is an excellent model gas for which detailed chemical mechanisms (both homogeneous and heterogeneous) are readily available in the literature but are not so complex as to make transient computations intractable. The inlet flow conditions are consistent with small scale power generation requirements while the inlet equivalence ratio is kept in a range to prevent the surface temperature from exceeding material property limits.

This paper examines the characteristics of both ceramic and metallic monolith substrates which differ significantly in thermophysical properties and hence have different operating requirements for startup. In commercial monoliths, the substrate material typically is coated with a catalytic washcoat, which depending on the amount of catalyst added (i.e. catalytic loading), may enhance the catalytic activity by increasing the available surface sites per unit length of the solid. The model accounts for catalytic loading by defining a parameter a* which, in effect, increases the geometric surface area per unit length available for catalysis. This parameter, which can enhance the amount of catalytic conversion, can account for the variety of catalyst loading conditions encountered in commercial monoliths.

II. Model Description

A. Overview

A complete description of the model is presented in Ref. 3 and only a top-level overview is presented here. The model is of a single catalytic channel unit (gas plus solid section) and represents an interior channel of a monolith that can be approximated as adiabatic. The single channel model is used to characterize the overall performance of the monolith. The model considers both the gas and solid phase of the channel. A premixed gas of fuel and air enters the channel at a prescribed velocity, temperature, and pressure. The model assumes that the channel is made of a solid substrate material (either ceramic or metal) which is coated with a thin catalytic material (washcoat). The combustion process considers both detailed gas phase and surface reactions. There is negligible pressure drop along the channel (i.e. no momentum equation solved) and the gas obeys the ideal gas law as shown in Eq. (1).

Equations (1)-(4) describe the gas-phase model which is quasi-steady relative to the transient solid, Eqs. (5)-(7), owing to the significantly longer heat-up times of the solid (~sec) compared with the residence times of the gas in the channel (~ msec) [3,4]. Equation (2) states that there is no net consumption of mass from the gas phase. In the gas-phase equations, heat and mass diffusion in the axial direction are neglected because the Peclet number based on typical gas velocities is much greater than unity. The model captures the heat transfer perpendicular to the flow using a heat transfer coefficient, h_T. In Eq. (3), if the reaction rate of species k due to catalytic reactions, $\dot{s}_k$, is greater than 0 (gas-species k desorbing from the surface) then the enthalpy of species k (h_k) is evaluated at the surface temperature ($T' = T_S$). For $\dot{s}_k < 0$ (gas-species k adsorbing to the surface), h_k is evaluated at the bulk gas temperature ($T' = T$).

There are K_g gas-phase species and the model uses two values of gas-phase species mass-fraction, a bulk flow value (Y_k) and a value adjacent to the catalytic surface but still in the gas phase (Y_{kW}). Lateral mass transfer coefficients come from the heat transfer coefficients using the analogy of heat and mass transfer[5]. The value of Y_{kW} comes from Eq. (5) which balances lateral mass transfer and the adsorption or desorption of species on the catalytic surface. Transport properties are mass averaged at each axial location at the bulk temperature.

Equation (6) shows the transient solid-phase energy equation which includes heat transfer to and from the gas inside the tube (term 2), heat generation terms due to catalytic reactions (terms 3 and 4), internal heat generation

(term 5), and axial heat conduction along the solid (term 6). The enthalpy of absorbing and desorbing gas species are evaluated just as described previously for the gas phase. For both gas and surface species, the enthalpy comes from data provided with the chemical mechanisms. Because the solid is thermally thin, the surface catalytic reactions (those involving surface species only) are modeled as surface heat generation in the solid. A prescribed volumetric heat generation (term 5) simulates Joule or external heating of the solid. The solid density, ρ_S, heat capacity, C_S, and thermal conductivity, k_S, are all constant in the model. The model accounts for varying surface coverage of adsorbed species. There are K_S total surface species including vacant surface sites. Equation (7) accounts for the time variation of surface species and assumes that the total number of active surface sites, Γ, remains constant. The value for Γ (=2.7063x10^{-5} mol / m^2 for platinum) comes from data provided with the heterogeneous mechanism.[8]

B. Equations

1. Gas phase

Equation of State:
$$\rho = \frac{P}{\left(R_U \diagup \overline{W}\right)T} \tag{1}$$

Overall mass-conservation:
$$\dot{m} = \rho u A = \text{constant} \tag{2}$$

Energy conservation:
$$\rho u A C_P \frac{\partial T}{\partial x} + A\sum_{k=1}^{Kg} \dot{\omega}_k W_k h_k + S\sum_{k=1}^{Kg} \dot{s}_k W_k \left[h_k(T) - h_k(T')\right] + h_T S\left[T - T_S\right] = 0$$
$$T' = \begin{cases} T & \text{if } \dot{s}_K \le 0 \\ T_S & \text{if } \dot{s}_K > 0 \end{cases} \tag{3}$$

Conservation for species k:
$$\rho u A \frac{\partial Y_k}{\partial x} = \dot{s}_k W_k S + \dot{\omega}_k W_k A \tag{4}$$

2. Surface and Solid-Phase Equations

Flux-matching at surface:
$$\rho h_{Dk}\left(Y_k - Y_{kW}\right) = -\dot{s}_k W_k \tag{5}$$

Energy conservation:
$$\rho_S C_S A_S \frac{\partial T_S}{\partial t} = h_T S\left(T - T_S\right) - S\sum_{k=1}^{K_g} \dot{s}_k W_k h_k(T') + S\sum_{k=1}^{K_S} \dot{s}_k W_k h_k(T_S)$$
$$+ \dot{q}_{gen} A_S + k A_S \frac{\partial^2 T_S}{\partial x^2} \tag{6}$$

Rate of change of surface site fractions:
$$\frac{\partial Z_k}{\partial t} = \frac{1}{\Gamma}\dot{s}_k \quad (k = 1 \ldots K_S) \tag{7}$$

3. Chemistry Expressions

$$\dot{\omega}_k = \sum_{i=1}^{n_g} \nu_{ki} q_i \tag{8}$$

$$\dot{s}_k = \sum_{i=1}^{n_S} \nu_{ki} q_i \tag{9}$$

$$q_i = k_{fi}\prod_{k=1}^{K}\left[X_k\right]^{\nu'_{ki}} - k_{ri}\prod_{k=1}^{K}\left[X_k\right]^{\nu''_{ki}} \tag{10}$$

The formulae for evaluating the gas-phase, $\dot{\omega}_k$, and surface, $\dot{s}_k$, reactions are shown in Eqs. (8)-(10) where q_i is the rate of the i^{th} reaction and ν is the stoichiometric coefficient. Formulas for the forward and reverse reaction rate constants may be found in the literature (for example, see Ref. 10). To account for an area enhancement due to the use of a thin catalytic washcoat, the geometric surface area per unit length, S, is multiplied by a surface area adjustment factor, a*, for terms dealing with surface reactions but not terms dealing with gas-to-surface transport. The parameter a* can also be thought of as the ratio of effective catalytic surface area to the geometric area. While a* is thought of here as a surface area enhancement, it is mathematically equivalent to modifying each kinetic pre-exponential term by the factor a*. In this study, a* is constant and set to a value of 20 which was previously shown to accelerate the kinetics sufficiently so that the reactions, once ignited, were mass-transfer limited.[3]

C. Solution Procedure

In general, the dependent variables (T, T_S, Y_k, Y_{kW}, and Z_k) as well as all the gas property values, transport coefficients, and reaction rate terms are functions of axial position and time. Since the gas phase is quasi-steady, it responds instantly to changes on the solid surface. Thus, the gas phase must be solved simultaneously with the changing solid phase and surface variables. This fact is especially important for cases which are mass-diffusion limited. The model separately integrates the gas-phase equations, Eqs. (3)-(4) which are ODEs, along the length of the reactor at specific time intervals. For this integration in x, the spatial distributions of the solid and surface parameters (T_S, Z_k, Y_{kW}, and $\dot{s}_k$) are fixed at the particular instant in time. The integration takes the necessary spatial step to handle stiff regions (i.e. ignition) interpolating the surface parameters, as necessary.

Equations (5)-(7) represent the surface / solid-phase equations and are directly coupled to the gas phase via the variables Y_k and T. The method of lines transforms Eq. (6) from a PDE into a system of ODEs. The solid is discretized into many control volumes; Equations (5)-(7) are written separately for each solid control volume thus forming a large system of ordinary differential-algebraic equations (DAE) for the solid.

The inclusion of detailed gas-phase and surface chemistry introduces numerical difficulty via mathematical stiffness. Stiffness in DAE systems essentially means that the time (or spatial) step required to solve the equations is much smaller than that required to obtain an accurate solution. Thus, stiff DAE systems require special numerical routines to solve them efficiently. The model uses the publicly available code DASPK[6], which is specifically designed for large systems of stiff equations, to perform the integrations.

The basic solution algorithm is to integrate the solid / surface equations, Eqs. (5)-(7), a finite amount forward in time, Δt, assuming that the axially varying gas-phase values are constant parameters during the interval Δt. The code, upon reaching Δt, integrates the gas-phase equations, Eqs. (3)-(4), along the length of the channel keeping the solid / surface values (T_S, Z_k, Y_{kW}, and $\dot{s}_k$) fixed. This method of solution essentially lags the gas phase by the amount Δt during the time integration. For the calculations presented in this paper, Δt was set to approximately 0.03 sec. (or about $1/100^{th}$ of a characteristic solid time scale based on interior gas-solid heat transfer time scale of ~3 sec. for the conditions in this paper) and provided time-accurate results. More details on the integration process are presented elsewhere.[3] The series of spatial and temporal integrations continued to steady state which was based on observing that the temperature profiles were no longer changing to within the numerical accuracy requested of the solution.

D. Chemistry

The fuel considered is carbon monoxide (CO) and includes both dry and wet versions – the wet version includes hydrogen chemistry which is used here to allow for the presence of water vapor in the feed stream. In the dry mechanism, the model tracks the following species: O, CO, O_2, CO_2, N_2, Pt(s), CO(s), CO_2(s), C(s), and O(s). The "(s)" denotes species adsorbed to the surface while the symbol Pt(s) denotes vacant sites on the platinum surface. With wet CO chemistry, the model also includes the following species: H_2, H_2O, H_2O_2, H, OH, HCO, HO_2, H(s), H_2O(s), and OH(s).

The gas-phase CO mechanism is from Davis et al.[7] For dry CO chemistry, the gas phase utilizes only steps 8, 21, and 23 of the mechanism – the remaining reactions deal with hydrogen chemistry and are neglected for dry CO computations. For calculations using wet CO chemistry, the full mechanism is utilized.

The heterogeneous reactions, which account for species adsorption, surface reactions, and desorption, come from a subset of a CH_4/O_2 on platinum mechanism proposed by Deutschmann et al. (the website version is used)[8]

Calculations for dry CO use steps 4, 5, 6, 7, 15, 16, 17, 18, 23, and 24 of the mechanism. For wet CO, all of the reaction steps are used except for steps 19-22 which involve the adsorption and subsequent decomposition of CH_4.

E. Thermophysical Properties and Geometric Parameters

For the gas phase, the thermodynamic properties (C_P and h_K) come from data provided with the mechanism. Transport properties come from the Gordon-McBride database or kinetic theory for pure species while the mixture uses appropriate mixing rules (see Ref. 3 for more details). For the solid, this paper presents calculation for 2 representative monolith reactors: one made of cordierite and the other from a metal alloy. Table 1 shows the solid-phase property variables used for the computations as well as the geometric parameters of the monolith (which are representative for the given material). The property values come from Appendix B of Ref. 9. While there is some variation in thermophysical properties of the solid with temperature (especially C_S and k_S), the computations used the constant values shown in Table 1 for these proof-of-concept calculations.

Table 1. Thermophysical and geometric parameters

Material	*Ceramic* Cordierite	*Metal* 70-80% Fe 10-20% Cr 5-10% Al
ρ_S, Density (kg/m^3)	2510	7400
C_S, Heat Capacity (J/kg/K)	1110	460
k_S, Thermal Conductivity (W/m/K)	2	19.4
d, Inner Diameter (mm)	1	1
A/A_T, Open Area Fraction per Monolith Cell	67%	88%
L, Monolith Channel Length (mm)	60	60

F. Initial and Boundary Conditions

The gas-phase equations, which are first-order, require only a single upstream boundary condition. The inlet conditions are representative of a flow downstream of a compressor in a small scale gas-power turbine. Specifically, the gas-phase boundary conditions upstream of the monolith are a temperature of 300K (in actual applications the temperature may be somewhat higher downstream of the compressor), a pressure of 3 atm., and a fuel equivalence ratio ranging from ϕ=0.1 to 0.4 using mixtures of CO and air. The channel flow velocities were either 5, 10, or 20 m/s and, because of the small channel diameter, the flow remained laminar. For the cases using wet CO chemistry, water vapor (1% by volume) is added to the inlet feed. The solid energy equation, Eq. (6), requires 2 boundary conditions due to the axial conduction term. There is heat loss to the inlet face of the monolith to the cold inlet gas. An estimate of the heat loss[3] comes from stagnation point theory which yields a $Nu_U \cong 33$, 47, and 66 for an upstream velocity of 5, 10, and 20 m/s, respectively, for the ceramic monolith geometry. For the metal monolith geometry, the upstream Nu_U is 62, 88, and 125, respectively. The outlet of the solid channel is adiabatic. During the back-end ignition phase, an externally applied heat source is imposed in the last 10% of the channel length for a specified time duration. This is implemented through the internal energy generation term, $\dot{q}_{gen}$, in Eq. (6).

The transient equations, Eqs. (6)-(7), require initial conditions for surface temperature and site fraction distribution along the length of the channel. The computations all began with a cold initial condition. The initial surface temperature is 300K while all surface sites are occupied initially by CO (i.e. surface site fraction $Z_{CO(S)}$ =1) owing to the higher sticking probability of CO relative to O_2, the 2 major reacting species in the flow. The initial condition for the remaining unknown, Y_{kW}, comes from an algebraic solution of Eq. (5).

In the numerical simulations, the internal heat-generation term, $\dot{q}_{gen}$, provides the energy to raise the monolith temperature to initiate catalytic reactions. The $\dot{q}_{gen}$ is either applied uniformly along the entire monolith or only across a portion of the monolith nearest to the outlet (termed back-end ignition). In both cases, heating by $\dot{q}_{gen}$ can simulate resistive heating in the solid. For the case of back-end ignition, $\dot{q}_{gen}$ can simulate heating by an external homogeneous flame that was established previously as shown in Fig. 1. In the simulations, $\dot{q}_{gen}$ is turned off after a given interval of time. In a real monolith, however, the homogeneous flame can continue to burn downstream of the monolith (in the after-bed space) provided that there is sufficient reactants (and high-enough gas temperature) even after catalytic reactions are established in the monolith.[11] Table 2 shows the parameters used in both the complete

reactor heating and the back-end ignition scheme. For back-end ignition, the ceramic required more energy deposited to reach an ignition temperature because of the ceramic's higher heat capacity.

Table 2. Ignition Parameters for Numerical Simulation

Ignition Strategy	$\dot{q}_{gen}$ *(W)*	*Duration (s)*
Heating Entire Monolith: ceramic & metal	30	1
Back-end Ignition (last 10% of length): Ceramic	3	1
Back-end Ignition (last 10% of length): Metal	3	0.4

III. Results

The results include both steady-state and transient data. The steady-state results include the fuel conversion as well as temperatures (both solid and gas) at the exit of the channel. For select cases, the species and temperature profiles along the channel are presented. The transient data presented is the propagation speed of the catalytic reactions front which can be used to gauge the preheat time of the channel.

A. Steady-state data

Figure 2 shows the fuel conversion (defined as the mass of gas-phase fuel reacted to the mass of gas-phase fuel fed into the reactor) at the outlet of the channel as a function of inlet equivalence ratio for the ceramic monolith. The calculations using the metal monolith produced very similar results in steady state and are not presented. In the figure, three separate computations are shown for each velocity: (1) complete monolith heating (labeled "All") with dry CO chemistry, (2) back-end monolith heating (labeled "Back") with dry CO chemistry, and (3) complete monolith heating using wet CO chemistry. In all cases, the internal heat generation was turned off after 1 second. As seen in Fig. 2, the model did not light-off (i.e. no steady conversion after removal of the heat source) for either heating profile at a $\phi \leq 0.1$. At $\phi = 0.11$, heating the entire monolith allowed light-off to occur and to be sustained resulting in fuel conversion at steady state. With heating the entire monolith, an increasing ϕ produced an increasing conversion with the largest increase (15% to 25%) occurring from $\phi = 0.11$ to 0.15. Between $\phi = 0.15$ and 0.4 there was only a modest 10-15% increase in total conversion.

For back-end ignition (dotted lines in Fig. 2), a higher ϕ of 0.15 was required to see sustainable conversion in the channel. From $\phi = 0.15$ to 0.23, the light-off position occurred at the channel exit and remained near the exit yielding only a small total conversion. For $\phi > 0.23$, the light-off position initially occurred at the outlet but subsequently propagated toward the inlet. In steady state, the resulting channel conversion for the cases which propagated (i.e. $\phi > 0.23$) matched that seen with complete channel heating.

In Fig. 2, the exit conversion decreased with increasing velocity. For instance, the conversion at $\phi = 0.4$ was 98%, 81%, and 51% for u = 5, 10, and 20 m/s. As the channel velocity increases from 5 to 20 m/s, the gas-phase residence time decreases from 12 ms to 4 ms, respectively. For a given channel diameter, the mass-transport time from the gas to the surface is more or less fixed (~2 ms for the present channel, see Ref. 3 and 4 for more discussion). Since the reactions are essentially mass-transfer limited in these cases, the faster velocity cases do not have enough residence time in the channel to completely react.

Figure 3 shows the solid-phase temperature (corresponding to the same calculations in Fig. 2) at the outlet of the monolith. At ϕ=0.1 and below, there is no light-off and the steady-state temperature is the ambient value of 300K. Above ϕ =0.1, the temperature at the end of the monolith increases with increasing ϕ. For complete monolith heating, the monolith's exit temperature ranges from ~650K at ϕ =0.11 to ~1630K at ϕ =0.4. Using back-end ignition, the channel exit temperature is ~100K lower compared to temperature achieved with complete monolith heating between ϕ =0.15 and 0.23. For $\phi > 0.23$, the catalytic reaction front propagated upstream and the steady-state solutions are the same irrespective of the heating profile. The temperature limits shown in Fig. 3 are taken from Ref. 9 and are exceeded for continuous operation with $\phi \geq 0.35$ for this particular monolith configuration.

Figure 4 shows the gas-phase temperature at the outlet of the monolith. The trends in this figure are the same as those seen in Fig. 3 except that the peak temperatures are somewhat less than the solid-phase since the gas is being

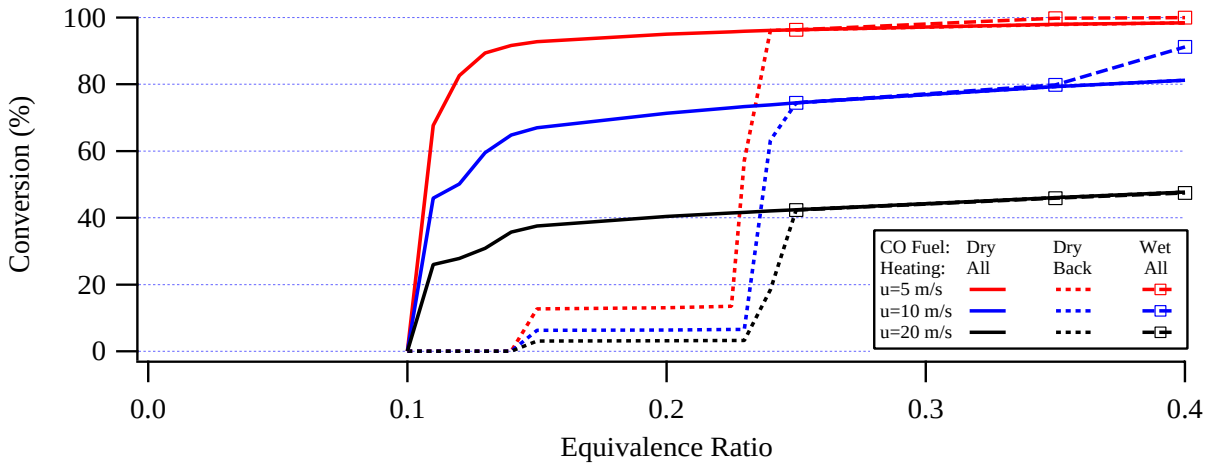

Figure 2. Steady-state fuel conversion through the ceramic monolith as a function of inlet equivalence ratio for a CO / air inlet feed. For the wet CO cases, water-vapor (1% by volume) is added to the inlet feed. Two different types of heating profiles are used in the simulation: complete monolith heating ("All") and back-end heating of the monolith ("Back").

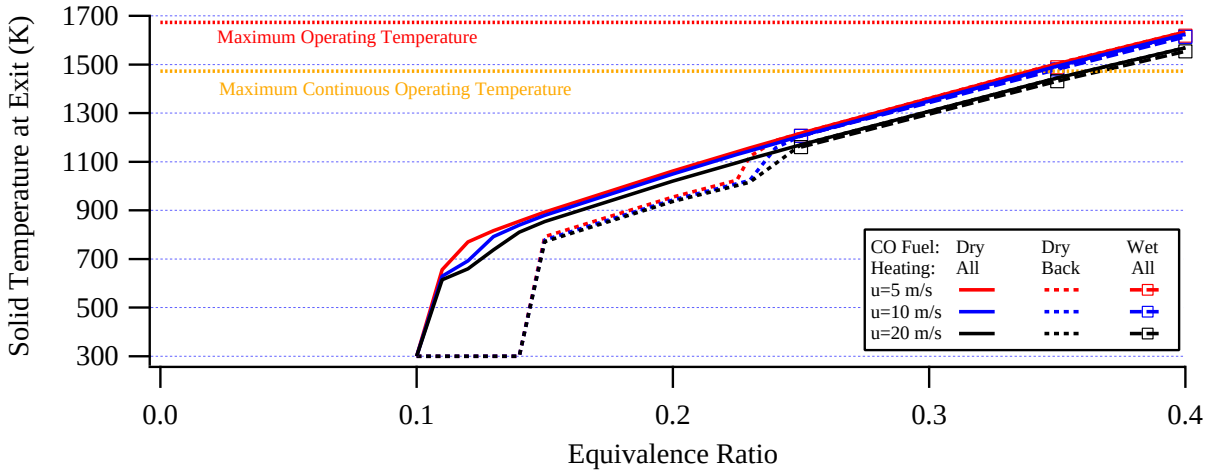

Figure 3. Steady-state solid temperature at the exit of the ceramic monolith.

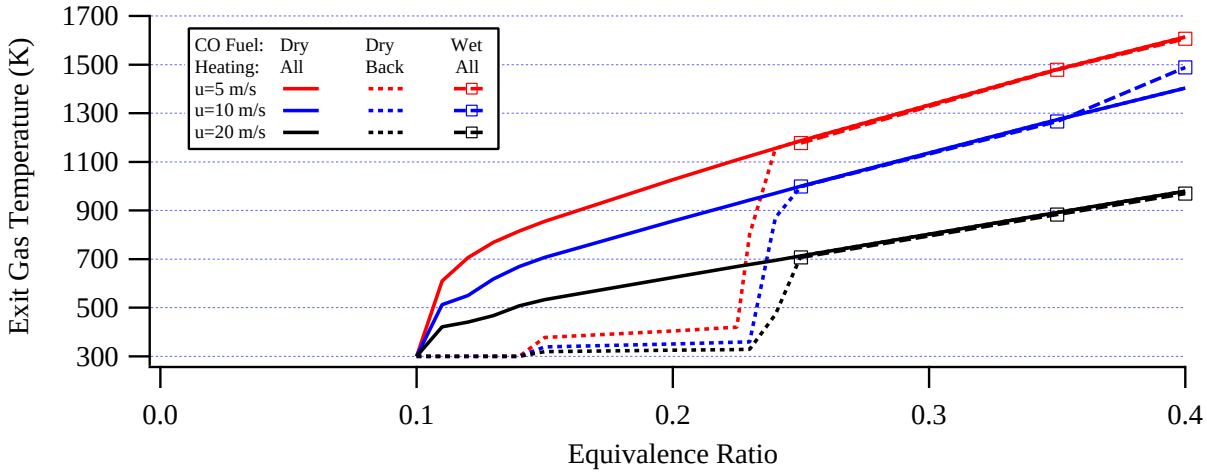

Figure 4. Steady-state gas-phase temperature at the exit of the ceramic monolith.

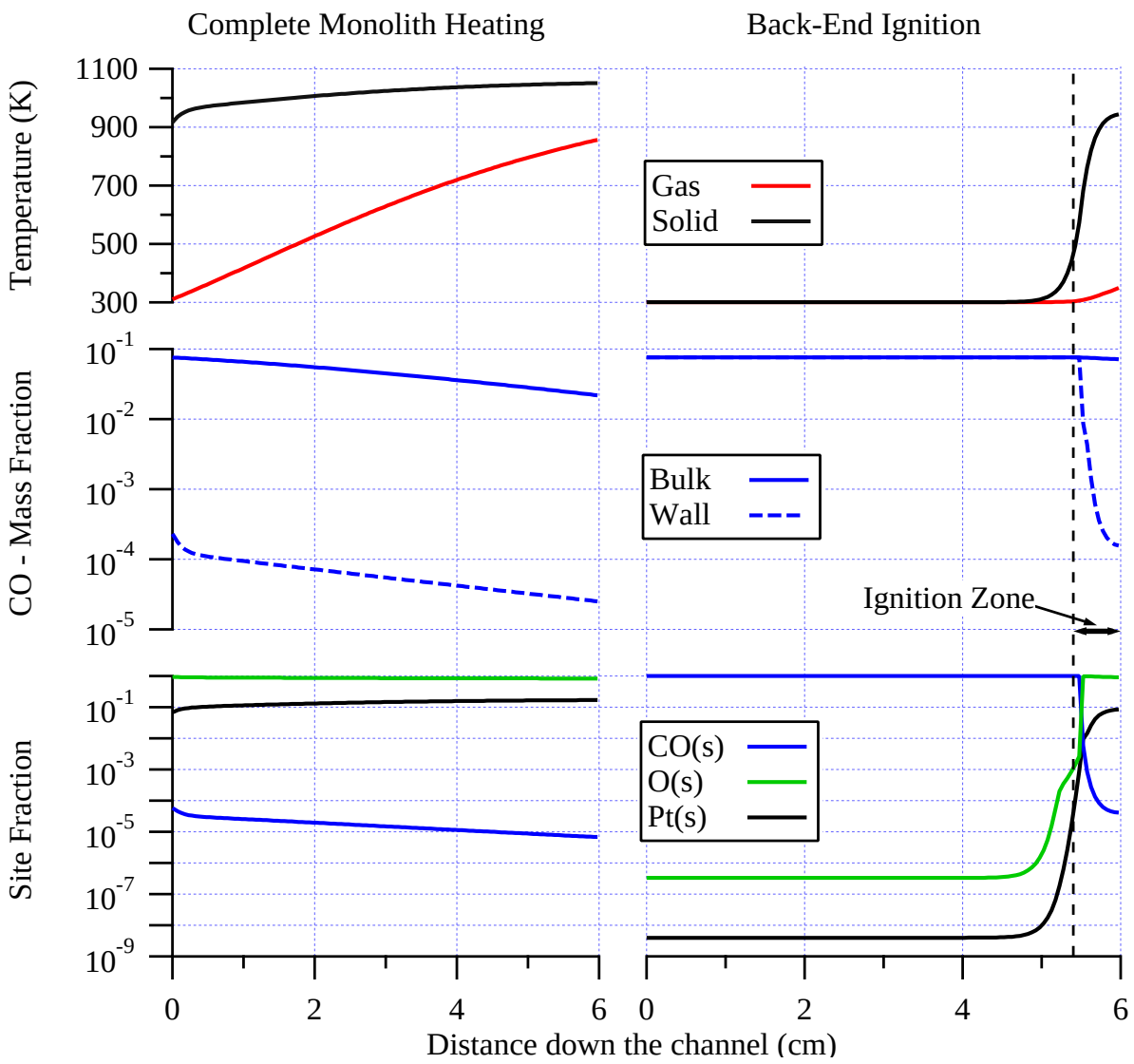

Figure 5. Steady-state temperature and species profiles along the length of the ceramic monolith channel after complete and back-end monolith heating. The inlet conditions are ϕ=0.2 at 10 m/s.

heated by the solid. For $\phi \geq 0.35$ and u=10 m/s, the computations using wet CO show a higher exit temperature (as well as a higher conversion as seen back in Fig. 2) compared with calculations using dry CO. In the wet CO case, gas-phase reactions have been initiated due to the presence of water vapor which provides hydroxyl (OH) radicals at the elevated temperatures. This particular condition is somewhat unique among the computations in that there is enough fuel remaining when gas temperatures become sufficiently high to initiate gas-phase reactions. For the u=20m/s, the residence time is too short to heat the gas-phase sufficiently for homogeneous reactions to occur. For the u=5m/s cases, the gas-phase temperatures near the outlet are sufficiently high at $\phi \approx 0.27$ and greater. In these cases, however, catalytic reactions have consumed most of the fuel, leaving little fuel for homogeneous reactions.

Figure 5 shows the steady-state temperature (top most graphs) and species profiles (middle and bottom graphs) along the length of the ceramic monolith. The inlet flow conditions are $\phi = 0.2$ at 10 m/s. At these conditions, two different steady states occurred depending on the monolith heating profile. For complete monolith heating (left column), significant catalytic reactions begin at the inlet as is evident by the high solid temperature and low CO mass-fraction (at the wall) exactly at the inlet. The solid-phase inlet temperature profile shows that there is upstream heat-loss given the non-zero temperature gradient at the inlet. The surface reactions are mass-transfer limited as is suggested by the large (almost 3 orders of magnitude) difference between the gas-phase bulk and wall mass-fractions for CO (reactions can be considered mass-transfer limited if there is a large difference between the bulk

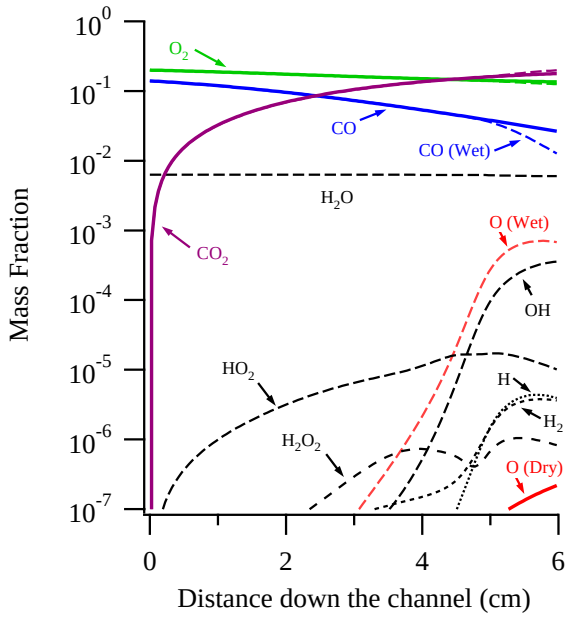

Figure 6. Steady-state mass-fractions comparing the dry and wet CO calculations at inlet conditions of ϕ=0.4 and u=10 m/s. The colored lines represent species in both the dry and wet CO computations. The hatched lines are only part of wet CO.

and wall values[9]). Regarding the surface species, O(s) is the major surface species in steady state with complete monolith heating.

For the case of back-end ignition (right column of Fig. 5), the catalytic reaction front anchors itself by the channel outlet near where the ignition energy was applied (see region labeled Ignition Zone in Fig. 5). In this case (ϕ = 0.2 at 10 m/s), the catalytic reaction did not propagate upstream. The solid-phase temperature near the outlet was over 900K but the gas was only slightly heated at the outlet (~ 350K) due to the short contact time with the hot surface. The wall-mass fractions of CO suggested that once catalytic reactions initiated, they became mass-transfer limited across only a short distance. For this case, the major surface species along the channel was CO(s) until the light-off point (x ≈ 5.5 cm). After light-off, the major surface species was O(s). These data suggest that up until light-off, the reaction is limited by the lack of O(s) on the surface. After light-off, the reactions appear to be limited by the low concentration of CO(s) on the surface which is likely a consequence of the slow transport rate (relative to the potential reactions rate) of gaseous CO to the surface.

For the ϕ=0.2 case shown in Fig. 5, the gas-phase temperature rises from 300K to 900K across the length of the channel was insufficient to trigger gas-phase reactions. Previously, Figs. 2 and 4 showed that for inlet conditions of ϕ=0.4 and u=10 m/s, there was a higher gas-phase exit temperature and greater CO conversion when comparing the dry and wet CO. For the wet CO cases, water vapor in the amount of 1% (by volume) was added to the inlet gas. Figure 6 shows the steady-state mass-fractions of the gas-phase species for the ϕ=0.4 and u=10 m/s calculations. The species common to both dry and wet CO calculations are shown in color. The species present only in the wet CO calculations are shown using hatched lines. For the dry CO calculations, only the major stable species are present in large quantities and there is very little O which indicates that no significant gas-phase reactions are occurring. The formation of CO_2 is due almost exclusively to surface reactions. For the wet CO calculations, the data in Fig. 6 show the presence of significant gas-phase radicals (especially O and OH) caused by the addition of water vapor in the inlet feed. The presence of water vapor (which introduces the OH radical) lowers the temperature required to initiate gas-phase reactions for CO / O_2 systems, as is well established in the combustion literature (for example, see Ref. 10). Comparing the bulk CO mass-fraction profiles (blue lines), it is clear from Fig. 6 that gas-phase reactions are causing further reduction of bulk CO (i.e. more conversion) in the wet CO calculations compared to the dry CO.

B. Transient Results

To this point, the results have shown that different steady states can occur depending on initial heating profile. With regard to back-end ignition, the cases of practical interest are those in which the catalytic reaction propagates upstream and heats the entire monolith. For these cases, a parameter of interest to the designer of catalytic monolith reactors is the heat-up time of the solid. Figure 7 shows the transient evolution of the solid-temperature (as well as the final steady state of both the solid and gas-phase temperature) for both a ceramic (left graph) and metal (right graph) monolith. The data in these figures correspond to inlet conditions of ϕ=0.4 and u=10 m/s and show both dry and wet CO computations using the back-end ignition scheme. For the ceramic monolith, the ignition term ($\dot{q}_{gen}$) was on for 1 second. For the metal monolith, the igniter duration was 0.4 seconds and was reduced to avoid unnecessarily high solid temperatures during the ignition process. Figure 7 shows that, just after removal of the heat generation term, the solid temperature was ~720K and 850K for the ceramic and metal monolith, respectively. It takes the reaction front about 78 seconds to propagate about midway across the channel for the case of a ceramic monolith and requires about 171 seconds to achieve steady-states conditions. For the metal monolith, it takes the

temperature front only 15 seconds to propagate half-way across the channel and only about 34 seconds to achieve steady state.

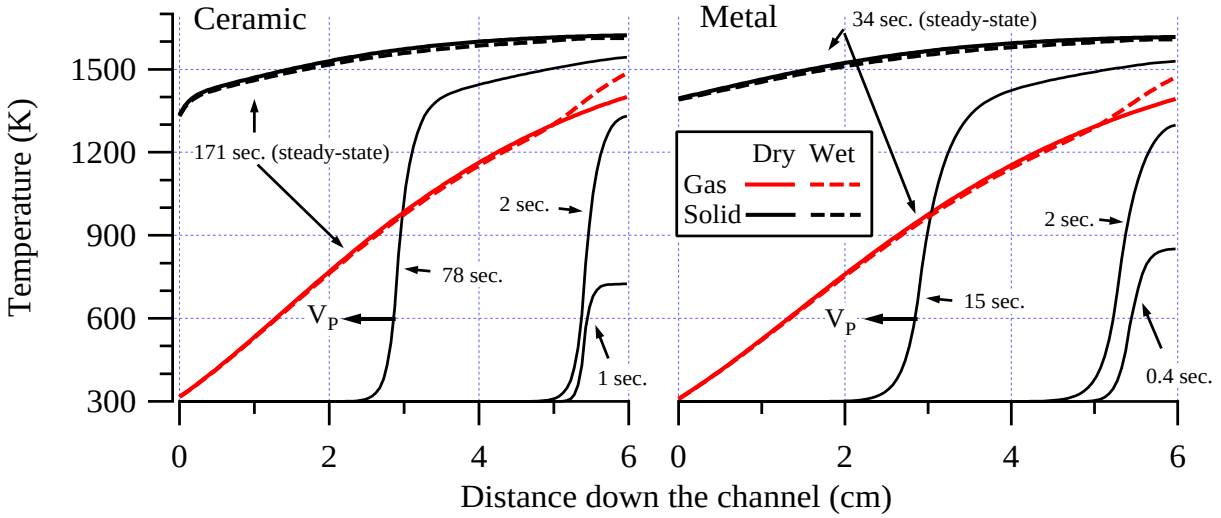

Figure 7. Transient evolution of the solid-phase temperature along the channel for both a ceramic (left graph) and metallic substrate (right graph). The computations are for an inlet condition of ϕ=0.4 and u=10 m/s and include both dry and wet CO cases.

The propagation velocity of the temperature front was nearly constant along the channel especially away from the ends of the channel. The temperature front was defined as the first location (starting from x=0) where the solid was 650K or greater. The propagation velocity, V_P, comes from a linear curve fit of the position versus time across the region from 25% to 75% of the propagation distance. The propagation distance was defined as the region between the location of the temperature front when the heat-generation was turned off (about x=5.5 cm in Fig. 7) and x=0.

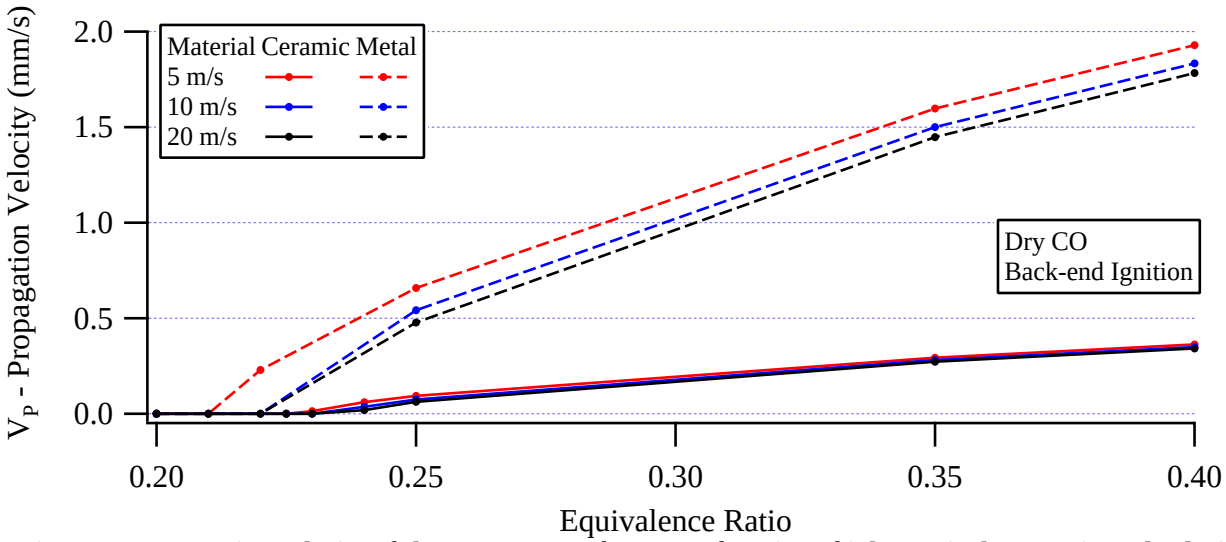

Figure 8. Propagation velocity of the temperature front as a function of inlet equivalence ratio and velocity during back-end ignition.

Figure 8 shows the propagation velocity of the solid-phase temperature front versus equivalence ratio for both the ceramic and metal monoliths. The propagation speed for the metal monolith is significantly higher than for the ceramic. For the ceramic monolith at a 10 m/s inlet velocity, the propagation speed of the reaction front ranged from V_P = 0.07 mm/s at ϕ=0.25 to V_P = 0.35 mm/s at ϕ=0.4 (with only slight variations with flow velocity). For the metal monolith at 10 m/s inlet velocity, the propagation speeds increased to V_P = 0.54 mm/s at ϕ = 0.25 and V_P =

1.83 mm/s at $\phi = 0.4$ (with slightly greater variations with flow velocity as shown in the figure). The propagation speed was roughly 7 times faster in the metal compared with the ceramic for the $\phi = 0.25$ cases. This ratio is close to the ratio of metal to ceramic thermal diffusivities (~8). For an equivalence ratio of $\phi = 0.4$, the propagation speed was about 5.25 times faster relative to the ceramic. The propagation speed ratios varied only slightly with inlet velocity. Interestingly, the equivalence ratio for which propagation occurred is not that different between the metal and ceramic monolith. The temperature front propagated at approximately ϕ=0.24 for the ceramic and only slightly leaner, ϕ=0.225, for the metal.

IV. Discussion

The data from the numerical simulations suggest that back-end ignition of a catalytic monolith for power generation devices is a feasible concept. With only a few watts of power (per channel) delivered to the back end of the monolith (say from a flame or resistive heating) to initiate localized catalytic reactions, the chemical energy released during the subsequent upstream propagation of the catalytic reactions can provide the remaining energy to heat the entire monolith. It is important for the reaction front to propagate upstream so that the solid temperature is hot along the majority of the channel. This allows the gas sufficient time to heat as it passes through the monolith which is the objective of the monolith (i.e. combustor) for power generation devices.

There is a reasonable range of equivalence ratios, about ϕ=0.25 to 0.35, for which back-end ignition and propagation occurred for the monolith configuration tested in the simulations. For this reaction, the lower ϕ corresponds to the minimum equivalence ratio for which propagation occurred while the highest ϕ corresponds to the material temperature limits. Since the data in this paper is specific to the monolith parameters used in the simulations, further work which can generalize when back-end ignition occurs is recommended. There is likely some combination of heat generation (due to catalytic reactions), heat-transfer to the flowing gas, and upstream heat conduction along the solid which allows the reaction front to propagate. Such a correlation would be valuable to the designer of a catalytic monolith reactor using the back-end ignition concept.

For a practical combustor using back-end ignition, the operating sequence can be more elaborate than tested in the simulations. During the ignition sequence, for instance, the inlet flow can be initially throttled back (e.g. the 5 m/s data) as well as operated under richer conditions. This may be important for establishing a downstream flame (such as shown schematically in Fig. 1) to avoid ignitability problems and blow-off. Once the catalytic reactions are initiated, the mixture can be made leaner to avoid exceeding any material property limits. In this situation, the downstream flame would eventually extinguish due to both the leaner inlet conditions as well as due to reactant consumption by the catalytic reactions. Once ignited and preheated, the operating range in terms of inlet equivalence ratio for the monolith reactor increases (e.g. down to almost ϕ=0.1 as demonstrated by the fully heated monolith cases).

Under certain conditions (ϕ=0.4 and 10 m/s as an example for the monolith configuration in the present work), gas-phase reactions can be initiated within the monolith. This can be an advantage since no further catalyst is required downstream of the onset of homogeneous reactions. The reaction can go to completion in the gas phase[11] reducing the length of the monolith which is advantageous from a cost and perhaps a design standpoint. Furthermore, limiting the length of the catalytic monolith prevents further heating of the solid if homogeneous reactions occur near the outlet. As a possible disadvantage, there is a risk of initiating homogeneous reaction too early within the monolith (if inlet conditions are mismanaged) potentially causing excessive temperatures downstream. Also, in many applications, the main emphasis of using a catalytic monolith is to avoid the high-temperatures of gas-phase reactions for both pollution control and material property limits in the power generation device. Fortunately, the data presented in this paper suggests that the onset of homogenous reactions occurs in only limited conditions and can be controlled with proper management of inlet conditions and monolith dimensions. We note that catalytically induced gas-phase reactions downstream of the monolith have been previously demonstrated experimentally.[11]

V. Conclusion

Using numerical simulations, this work demonstrates a concept called back-end ignition for lighting-off and heating a catalytic monolith in a power generation system. This concept uses a heat source (e.g. a flame) or resistive heating in the downstream portion of the monolith initiating a localized catalytic reaction which subsequently propagates upstream, heating the entire monolith. The simulations used a transient numerical model of a single catalytic channel. This channel represents an interior channel of the monolith which is approximated as adiabatic and is used to characterize the behavior of the entire monolith. The model treats both the gas and solid phases and

includes detailed homogeneous and heterogeneous reactions. The simulations used chemical mechanisms of both dry and wet CO and air mixtures as a model fuel for the proof-of-concept calculations. The solution procedure takes advantage of the slow solid time constants relative to the gas phase allowing the use of a quasi-steady approximation for the latter. An important parameter in the model for back-end ignition is upstream heat-conduction along the solid.

Back-end ignition occurred using both a ceramic and metal monolith, with the heat-up times significantly faster for the metal monolith. In some cases, back-end ignition occurred without upstream propagation. For an inlet velocity of 5 m/s at 3 atm., back-end ignition occurred at $\phi \geq 0.15$ but propagation of the reaction front required a richer inlet equivalence ratio ($\phi \geq 0.24$). For both the higher inlet velocities tests (10 and 20 m/s), slightly richer conditions ($\phi \geq 0.25$) were required for upstream catalytic propagation. The propagation speed of the reaction front along the metal monolith ranged from about 0.5 to 1.8 mm/s (with some variation with inlet velocity) for ϕ=0.25 and 0.4, respectively. For the ceramic monolith, the propagation velocities were significantly slower ranging from ~0.05 to 0.36 mm/s for the same equivalence ratio range. Once light-off and propagation occurred, the inlet equivalence ratio could be reduced significantly (e.g. $\phi \approx 0.11$) and still maintain an ignited monolith as demonstrated by calculations using complete monolith heating.

Under certain conditions (ϕ=0.4 and 10 m/s as an example for the monolith configuration in the present work), gas-phase reactions were predicted to occur at the back end of the monolith. In these computations, significantly more CO conversion occurred with the presence of water vapor (1% by volume) in the inlet feed. The water vapor introduced the OH radical which subsequently lowered the temperature required to initiate gas-phase reactions with CO and air. Besides having OH radicals and high enough gas-phase temperatures, sufficient fuel must remain in the gas phase to initiate gas-phase reactions. At long residence (slower inlet velocities), catalytic reactions alone can consume most of the fuel in the reactor.

Acknowledgments

The authors gratefully acknowledge support from NASA to the National Center for Space Exploration Research (NCSER) and Case Western Reserve University (CWRU) under Cooperative Agreement NNC04AA29A.

References

[1] Struk, P.M., Dietrich, D.L., Mellish, B.P., Miller, F.J., and T'ien, J.S., "Catalytic Ignition and Upstream Reaction Propagation in a Platinum Tube," *Proceedings of the 2006 Technical Meeting of the Central States Sections of the Combustion Institute,* Cleveland, Ohio, May 21-23, 2006.

[2] Miller, F.J., Mellish, B.P., Struk, P.M., Dietrich, D.L., and T'ien, J.S., "Propagating Flames and Acoustic Instabilities in Tubular Microcombustors," *Proceedings of the 2006 Technical Meeting of the Central States Sections of the Combustion Institute,* Cleveland, Ohio, May 21-23, 2006.

[3]Struk, P., M., "Modeling of Catalytic Channels and Monolith Reactors," Ph.D. Dissertation, Mechanical and Aerospace Engineering Dept., Case Western Reserve University, Cleveland, OH, 2007.

[4] T'ien, J.S., "Transient Catalytic Combustor Model," *Combustion Science and Technology,* Vol. 26, No. 1-2, 1981, pp. 65-75.

[5]Incropera, F.P., and Dewitt, D.P., *Fundamentals of Heat and Mass Transfer*, 3rd ed., John Wiley and Sons, New York, 1990.

[6]Brown, P.N., Hindmarsh, A.C., and Petzold, L.R., "Using Krylov Methods in the Solution of Large-Scale Differential-Algebraic Systems," *Siam Journal on Scientific Computing*, Vol. 15, No. 6, 1994, pp. 1467-1488.

[7]Davis, S.G., Joshi, A.V., Wang, H., and Egolfopoulos, F., "An optimized kinetic model of H2/CO combustion," *Proceedings of the Combustion Institute*, Vol. 30, No. 1, 2005, pp. 1283-1292.

[8]Deutschmann, O., Schmidt, R., Behrendt, F., and Warnatz, J., "Numerical Modeling of Catalytic Ignition," *Proceedings of the Combustion Institute*, Vol. 2005, No. 11/1, 1996, pp. 1747-1754, URL: http://www.detchem.com/mechanisms/ [cited November 1, 2006].

[9]Hayes, R.E., and Kolaczkowski, S.T., *Introduction to Catalytic Combustion*, Overseas Publishers Association, Amsterdam, 1997, pp. 654-655.

[10]Kee, R.J., Coltrin, M.E., and Glarborg, P., *Chemically Reacting Flow Theory & Practice*, John Wiley & Sons, Inc., Hoboken, NJ, 2003.

[11]T'ien, J. S. and Anderson, D. N.: "Gas Phase Oxidation Downstream of a Catalytic Combustor," NASA TM-81551 (1979).